



# Effect of Nb Addition on the Thermodynamic of Solidification in a Ti-Ni-Cu Alloy

Jessica Dornelas Silva<sup>a\*</sup> , Dilson Silva dos Santos<sup>b</sup> , Leandro de Arruda Santos<sup>a</sup> ,

Vicente Tadeu Lopes Bueno<sup>a</sup> 

<sup>a</sup>Universidade Federal de Minas Gerais (UFMG), Departamento de Engenharia Metalúrgica e de Materiais, Belo Horizonte, MG, Brasil.

<sup>b</sup>Universidade Federal do Rio de Janeiro (UFRJ), Departamento de Engenharia Metalúrgica e de Materiais, Rio de Janeiro, RJ, Brasil.

Received: December 16, 2022; Revised: March 25, 2023; Accepted: May 21, 2023

The solidification process of  $Ti_{52-x}Ni_{38}Cu_{10}Nb_x$  alloys was evaluated using the CALPHAD method and microstructural analyses of as-cast alloys with Nb additions of  $x = 4, 6, 8$  and  $10$  at%. Both in Scheil calculator and structural analyses, the observed phases were TiNi,  $\beta$ -Nb/Ti, and  $Ti_2Ni$ . TiNi is the matrix phase, and it presented similar amounts of Ti and Ni with varying Nb contents. Enrichments of Ti content and depletion of Ni are expected in the liquid with the solidification of this phase. Formation of  $Ti_2Ni$  and  $\beta$ -Ti is related to the excess of Ti. Increasing Nb content hinders the formation of  $Ti_2Ni$ , favoring  $\beta$ -Ti. In turn, Ni depletion and Nb accumulation led to the TiNi/ $\beta$ -Nb eutectic. In the intermetallic phases, coherent ratios were obtained when Cu was considered a substitute for Ni, and Nb, for Ti.

**Keywords:** TiNiCu-based alloys, shape memory alloy, solidification, Scheil calculator.

## 1. Introduction

Shape memory alloys (SMAs) are functional materials capable of recovering from strains larger than the elastic limits, presenting shape memory effect (SME) and superelasticity (SE). These properties are related to the occurrence of a reversible martensitic transformation (MT) from a high temperature austenitic phase to a low temperature martensitic phase. When stresses are applied to the material in the martensitic state, deformation is produced by the reorientation of martensitic variants. The initial shape is recovered by promoting the reverse transformation to austenite through proper stimulus. In conventional SME, it is achieved by heating the deformed material to a temperature above the austenitic finishing temperature,  $A_f$ . When the SMA is deformed in the austenitic stability region, i.e., in temperatures higher than  $A_f$ , the martensitic transformation is induced by tension. In this case, the reverse transformation occurs simply by unloading the SMA, recovering the initial shape and achieving  $SE^{1-3}$ .

The reversible MT is characterized by the presence of thermal and stress hysteresis. In thermal cycles, the direct transformation occurs during cooling, starting at  $M_s$  and finishing at  $M_f$  temperatures. During heating, the reverse transformation starts and finishes at  $A_s$  and  $A_f$ , respectively. In mechanical cycles, the induced and reverse transformations occurring during loading and unloading, respectively, take place at different stress plateaus. The length of the transformation hysteresis depends on the crystallographic compatibility between austenite and martensite and the amount of crystallographic defects generated during thermal and mechanical cycling<sup>4,6</sup>.

Ternary TiNiCu SMAs are characterized by narrow thermal and stress transformation hysteresis due to a decrease in friction against the movement of the interface between austenite and martensite<sup>7,8</sup>. These characteristics can be associated with improved structural and functional fatigue properties of SMAs<sup>9-12</sup>. Used in actuation and damping applications, TiNiCu alloys present low composition and heat-treatment sensibility, and usually SME at room temperature. However, they present brittle behavior when amounts higher than 10at% Cu are added<sup>1,13</sup>.

When adding Cu in binary TiNi as a substitute for Ni in TiNiCu SMAs, the B2 CsCl-type TiNi intermetallic remains the primary phase with additions of up to 30at% Cu, with Cu dissolved in Ni's atomic site. This is the austenitic phase that undergoes reversible MT and, thus, is responsible for the SME and  $SE^{1,7,8}$ .  $Ti_2(Ni,Cu)$ ,  $Ti(Ni,Cu)_2$ , CuTi second-phases have been reported in the as-cast microstructure of TiNiCu SMAs<sup>14-18</sup>. In different chemical composition ranges, FCC (Ni), BCC (Ti),  $Ni_3Ti$ ,  $CuTi_2$  as well as  $T_1(TiNiCu)$ ,  $T_4(Ti_5Ni_4Cu)$  and  $T_6(TiNi_2Cu)$  ternary phases can also be formed from the liquid<sup>19</sup>. Assessments of ternary Ti-Ni-Cu are available in Ref<sup>20,21</sup>.

The addition of Nb to TiNiCu alloys has been related to an increased ductility due to the presence of a Nb-rich ( $\beta$ -Nb) phase<sup>22</sup>. Moreover, heat-treatment sensibility and high cycling stability have been reported in alloys with decreased transformation temperatures<sup>22-25</sup>. In this manner, there is a potential to develop heat-treatable and formable alloys that present high functional and mechanical stability for room temperature applications that require SE.

In previous study<sup>26</sup>, the effect of Nb on the phase stability in  $Ti_{52-x}Ni_{38}Cu_{10}Nb_x$  alloys was evaluated.

\*e-mail: [jdornelas@ufmg.br](mailto:jdornelas@ufmg.br)

The as-cast phase constitution could not be predicted on conventional thermodynamic calculations, being related to chemical segregations during solidification. However, the metastable second phases presented high stability during homogenization treatment. In this study, we aim to use the CALPHAD method employing the Scheil calculator in association with experimental microstructural and semi-qualitative chemical analysis (EDS) to provide further understanding on the development of different phases during solidification of TiNiCuNb alloys.

## 2. Experimental Procedure

Ti<sub>52-x</sub>Ni<sub>38</sub>Cu<sub>10</sub>Nb<sub>x</sub> alloys with Nb additions of x = 4, 6, 8 and 10 at% were produced from elemental constituents (>99.5% purity) into 30 g ingots by arc-melting using 250-300 mA in a water-cooled copper mold. Samples were remelted at least six times to promote chemical homogeneity. The cast alloys will be hereafter referred as Nb4, Nb6, Nb8 and Nb10, according to the alloy's Nb content.

X-ray diffraction (XRD) was used for phase identification in a Panalytical Empyrean diffractometer with Cu-K $\alpha$  radiation and a scan speed of 0.02°/s. The microstructure of the as-cast alloys was evaluated by scanning electron microscopy (SEM – FEI Inspect and FEI Quanta 3D FEG) using backscattered electrons. EDS mapping and punctual analyses were performed to provide a comparative analysis on the solute distribution within different phases.

Solidification and thermodynamic calculations were performed using the CALPHAD method on ThermoCalc® employing TCNI8 – v8.1 database. Scheil-Gulliver solidification simulation is based on the assumption that mixing of all elements is effective in the liquid while no diffusion occurs in solid phases. Thermodynamic equilibrium is considered in the liquid/solid interface. The use of this method allows to consider the solute redistribution during solidification, which can provide insights on how solute segregation leads to the formation of out-of-equilibrium phases<sup>27-29</sup>. Some examples of the use of this method to describe the solidification behavior in various systems can be found in Refs<sup>30-33</sup>. In this study, variations in the liquid composition during solidification were obtained using Scheil calculator. The equilibrium calculator was used to assess equilibrium, considering the chemical segregation that generates different phases during solidification as measured by Scheil calculations and EDS element distribution through phases formed at different stages of solidification.

## 3. Results and Discussions

### 3.1. Computational thermodynamic analysis

The alloy's microstructures and the effect of Nb were assessed in Ref<sup>26</sup>, where microstructural images and XRD patterns can be obtained. TiNi, Ti<sub>2</sub>Ni and  $\beta$ -Nb phases were identified in all the cast alloys, while metallic Ti was present in Nb10. TiNi is the matrix phase;  $\beta$ -Nb appeared mainly in a eutectic constituent with TiNi; Ti<sub>2</sub>Ni presented geometric and dendritic-like morphologies, frequently associated with  $\beta$ -Nb and the eutectic constituent; and metallic Ti appeared mainly as dendrites.

This microstructure constitution was pointed out to be in qualitative agreement with results obtained from the Scheil solidification calculator<sup>26</sup>, represented in Figure 1a with the addition of results for Nb8. It is expected that solidification starts with the formation of TiNi and finishes with the formation of Ti<sub>2</sub>Ni and  $\beta$ -Nb.

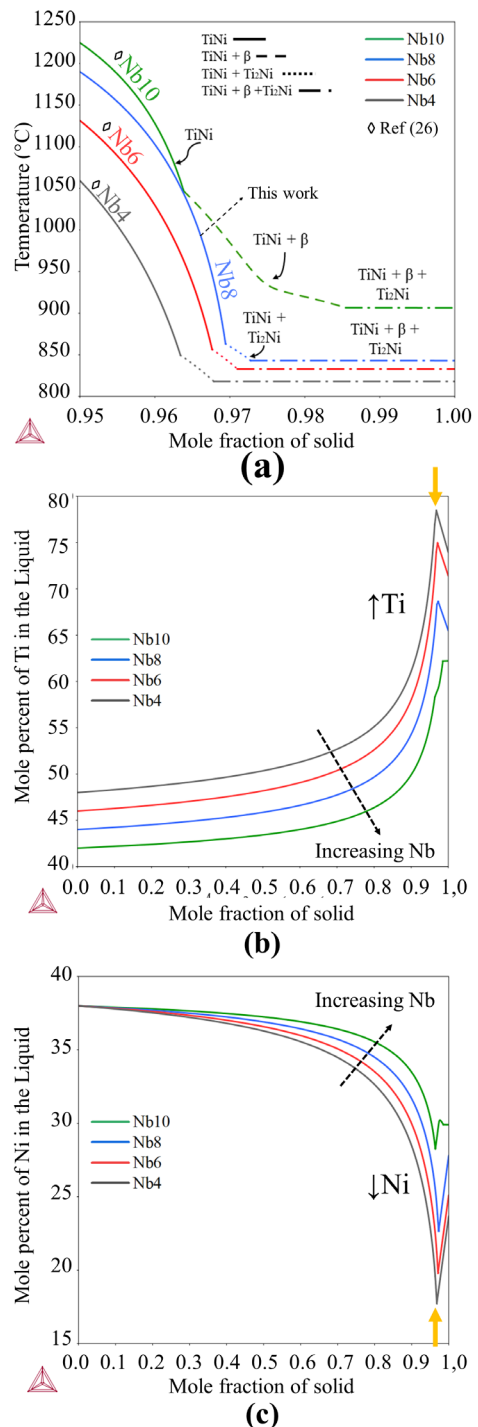


**Figure 1.** (a) Solid-phases in equilibrium with the liquid as a function of temperature and mole fraction of solid adapted from Ref<sup>26</sup>, and variations of (b) Ni and (c) Ti contents in the liquid as a function of mole fraction of solid obtained via Scheil calculator.

Variations on the amount of Ni and Ti in the liquid phase during solidification are presented in Figure 1b and 1c, respectively. When the TiNi matrix is formed, enrichments on the Ti content concurrent to decreases on Ni's were observed in all compositions. The composition profile changes in the final steps of solidification, with the formation of second phases, as indicated by full arrows. The calculated chemical gradient of these two elements on liquid are greater with decreasing Nb content, and the second-phase development is favored in the alloy with the highest Nb percentage.

In Figure 2, pseudobinaries of the Ti-Ni phase diagram with fixed amounts of 4at% Nb and 10at% Nb are plotted. From Scheil calculations, solidification leads to chemical variations on the liquid as indicated by arrows in the region of excesses of Ti in relation to Ni. In the phase diagram with fixed 4at% Nb (Figure 2a), a three-phase field containing TiNi,  $Ti_2Ni$  and liquid is observed after the two-phase liquid + TiNi field. The presence of the Ti-rich  $Ti_2Ni$  intermetallic in equilibrium with the liquid may be associated with its dendritic morphology in Nb4 alloy (II in the inset of Figure 2a).

In the 10at%Nb phase diagram (Figure 2b), a TiNi,  $\beta$  and liquid region is observed instead. The  $\beta$  phase presents varying amounts of Ti and Nb, depending on the temperature and composition: Ti-rich solid solutions are favored at high temperatures and Ti enrichments. Hence, it appears that Nb decreases the stability region of  $Ti_2Ni$ , favoring the solidification of  $\beta$ -Ti dendrites in Nb10 (II in the inset of Figure 2b).

In both diagrams (Figure 2), solidification finishes in a TiNi +  $\beta$  +  $Ti_2Ni$  field, leading to the simultaneous formation of these phases. At temperatures lower than 800°C, TiNi +  $\beta$ -Nb +  $Ti_2Ni$  are in equilibrium within a large

range of compositions, which could be responsible for their high stability during heat-treatments. In turn,  $\beta$ -Ti is only stable at high temperatures, which could explain the partial dissolution previously observed<sup>26</sup> during heat-treatment. In this manner, it can be noted that the solidification sequence and developed phases are intimately related to the TiNiNb system.

### 3.2. Solute distribution

The distribution of elements in the different alloys obtained by EDS mapping is presented in Figure 3. Semiquantitative results obtained by punctual analyses are presented in Figure 4. The presence of Ti can be highlighted in  $Ti_2Ni$  and  $\beta$ -Ti while lower fractions are observed in the  $\beta$ -Nb phase, as pointed out, respectively, by white and yellow arrows in Figure 3b. Ni is mostly present in the TiNi matrix, where heterogeneities can be noted by the impoverishment of this element in regions adjacent to the  $\beta$ -Nb phase and the eutectic constituent, as pointed out in Figure 3c. These same regions presented excesses of Cu (Figure 3d). This element, which is always present as a solute, is mostly dissolved in the eutectic, preferably in the TiNi phase as evidenced in Figure 4c. In turn, low solubility is observed in the Ti-rich second phases. Nb is mainly present as the  $\beta$ -Nb phase (Figure 3e), where Ti was the main solid solution atom (Figure 4a). The presence of the eutectic constituent with  $\beta$ -Nb phase and the concentration of Nb indicate an accumulation of Nb on the liquid in the final stages of solidification.

From the punctual analyses (Figure 4), it can be observed that TiNi, the primary phase formed during solidification, presented similar amounts of Ti (Figure 4a) and Ni (Figure 4b) in alloys with varying Nb contents. In the eutectic constituent, mean fractions of 27-31 at% of Ni and 40-43at% Ti were measured.

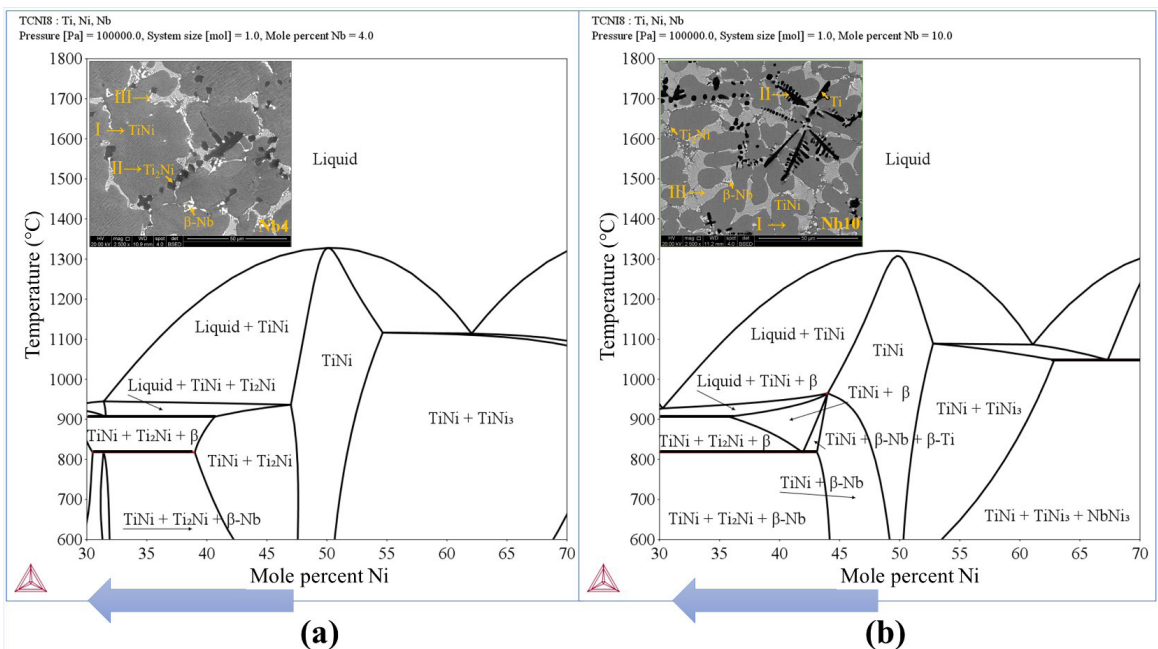
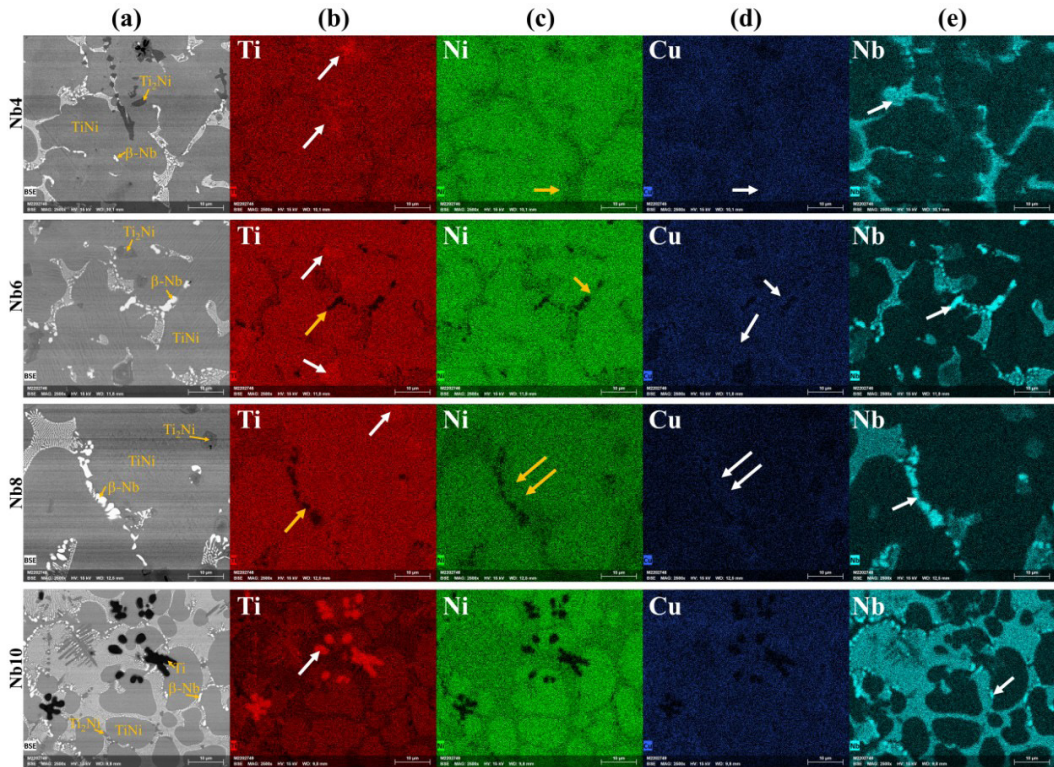
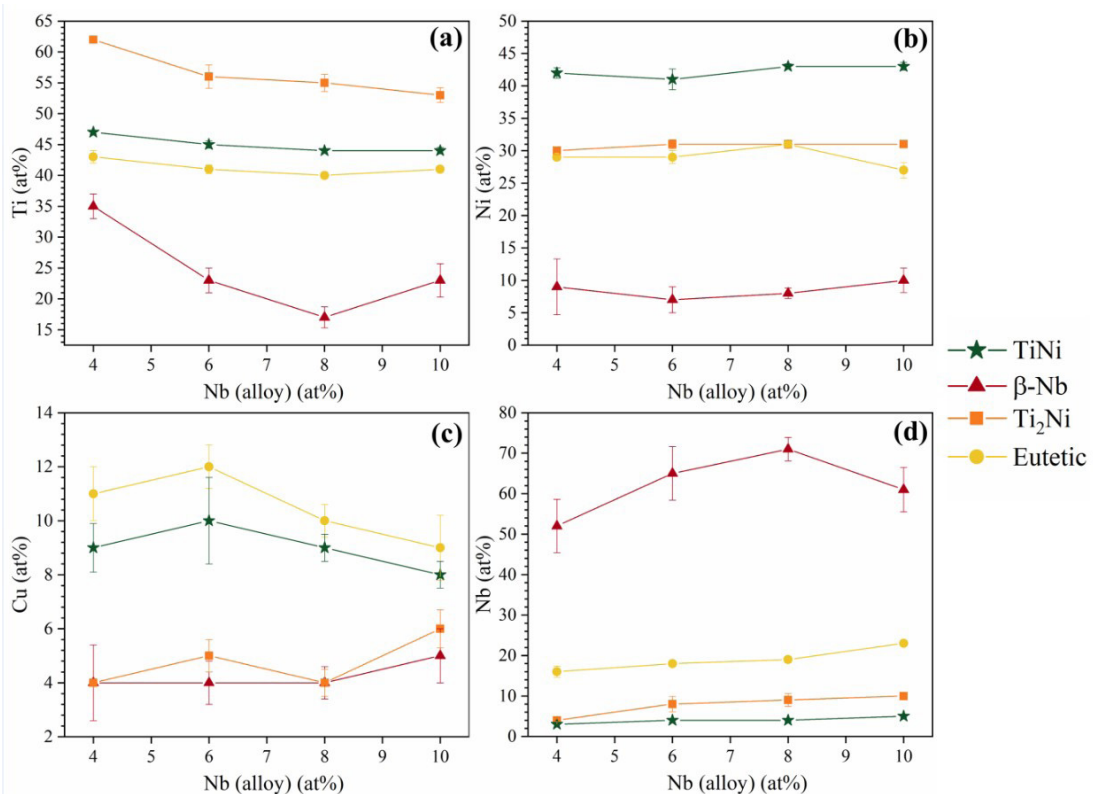


Figure 2. TiNi pseudobinaries with fixed amounts of (a) 4 at% Nb and (b) 10 at% Nb.





**Figure 3.** EDS mapping in (a) Nb4, Nb6, Nb8 and Nb10 microstructures showing the distribution of (b) Ti, (c) Ni, (d) Cu and (e) Nb.



**Figure 4.** Mean contents of (a) Ti, (b) Ni, (c) Cu, and (d) Nb in different phases and the eutectic as a function of Nb content of the alloy measured by semiquantitative EDS analysis.

The mean mole fraction of Nb (Figure 4d) in this constituent varied from 16at% to 23at%, increasing with increasing Nb content in the alloy. Virtually equal amounts of Ni have been observed in the eutectic constituent and the  $Ti_2Ni$  phase, Figure 4b, formed in the final steps of solidification. This may indicate that they form simultaneously when the Ni content in the liquid reaches a critical value. This agrees with Scheil calculation results, which shows the depletion on the Ni content of the liquid with an inflection point when second phases are formed.

In turn, measured Nb-contents in the eutectic constituent indicate that there is a Nb accumulation in the liquid. Hence, the relationship between diminishing Ni and increasing Nb was assessed by a Ni-Nb pseudobinary calculation with fixed amounts of Ti and Cu as the base alloy (52at% and 10at% respectively), plotted in Figure 5. It can be observed that the diminishing Ni is sufficient for the formation of the eutectic involving  $\beta$ -Nb, even with constant Ti and Cu contents. When the Nb content of the alloy is higher, and hence, a higher enrichment of Nb on liquid is expected, the eutectic reaction involving NiTi and  $\beta$ -Nb occurs at higher temperatures and the formation of  $\beta$ -Nb is favored. On the other hand,  $Ti_2Ni$  is only an equilibrium phase in poor Nb content regions. This means that they could either be formed at earlier stages of solidification in alloys with low Nb additions, such as Nb4, or through the partition of Ti and Nb in the final stages.

Ratios of mean elements contents in each intermetallic phase were assessed to evaluate stoichiometry fits. As it can be observed from Figure 6, coherent ratios are obtained in TiNi when Cu is considered a substitute for Ni, and Nb, for Ti. In  $Ti_2Ni$ , the calculated ratio fits the stoichiometry best when only Nb is considered a substitute for Ti. These results are endorsed by previous observations that Nb occupy Ti sites in Ni-Ti intermetallic phases on Ni-Ti-Nb ternary<sup>34</sup>.

### 3.3. Solidification of the cast alloys

Based on Scheil calculations, pseudobinary equilibrium extrapolations and EDS results discussed in the previous sections, it is proposed that solidification occurs as follows (Figure 7). The TiNi matrix phase is formed, and the calculated liquid composition as a function of the fraction of solid phase indicated enrichments on the Ti and decreases on the Ni contents (Figure 7b). This leads to the formation of Ti-rich second-phases,  $Ti_2Ni$  and  $\beta$ -Ti (Figure 7c). Increasing alloy's Nb-content jeopardizes the formation of  $Ti_2Ni$  and favors de formation of  $\beta$ -Ti at high temperatures, as the  $\beta$ -phase is stabilized from the liquid in Ti-rich regions of the TiNi-Nb pseudobinary phase diagram (Figure 2).

The decrease in the Ni content and accumulation of Nb in the liquid (Figure 5) are associated with the formation of the eutectic involving  $\beta$ -Nb (Figure 7d). The simultaneous formation of TiNi,  $\beta$ -Nb and  $Ti_2Ni$  at the final stages of solidification appears to occur when a critical Ni content is reached (Figure 7e). The other elements partition within the formed phases:

Ti-rich regions become  $Ti_2Ni$  while Nb-rich regions turn into the eutectic, where Cu is preferably in TiNi's lamellae.

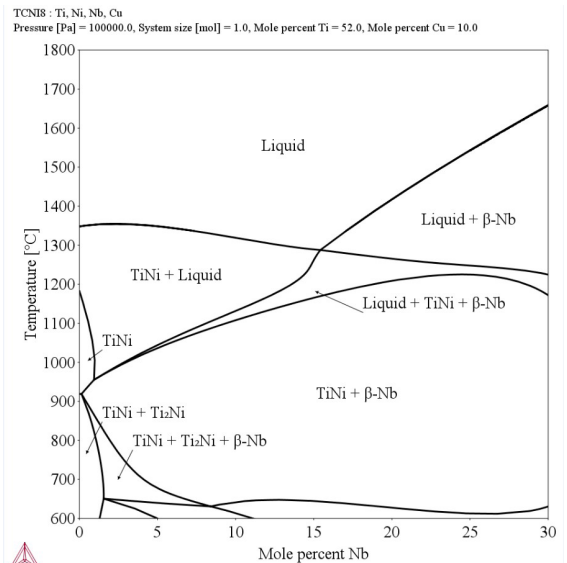


Figure 5. Effect of increasing Nb and diminishing Ni in Ni-NbTi<sub>52</sub>Cu<sub>10</sub> pseudobinary.

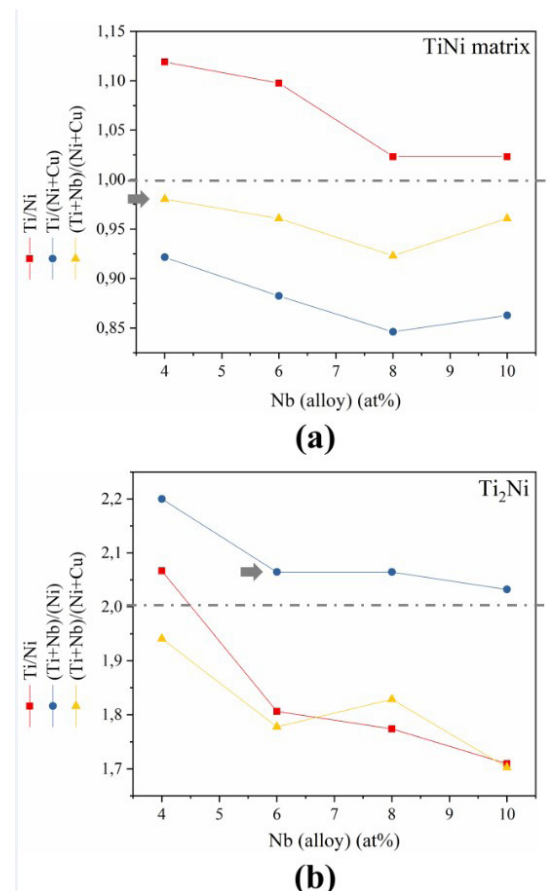


Figure 6. Measured element ratios in (a) TiNi and (b)  $Ti_2Ni$  intermetallic.

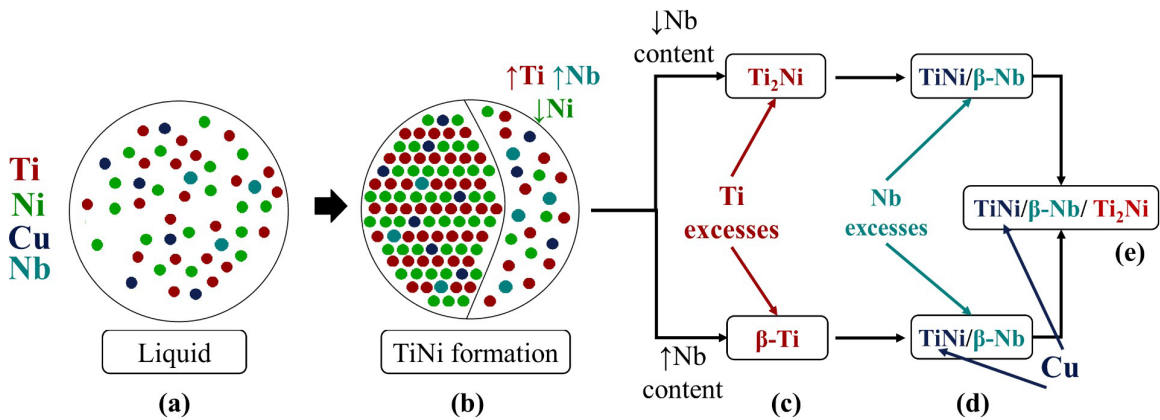


Figure 7. Proposed solidification scheme of the produced TiNiCuNb alloys.

#### 4. Conclusions

Solidification of TiNiCuNb alloys were evaluated from the perspective of thermodynamic simulations associated with experimental microstructural analyses. For that, TiNiCuNb alloys were produced by arc-melting and the resultant microstructure was evaluated. Thermodynamic simulations were performed using conventional equilibrium and Scheil calculators. TiNi, β-Nb and Ti<sub>2</sub>Ni were observed in the as-cast microstructure and in the Scheil calculation for all the studied alloys.

It was proposed that solidification starts with the formation of TiNi, and excesses of Ti and Nb remain in the liquid while Ni is consumed. The amount of Ti and Ni in TiNi doesn't vary significantly within alloys of different Nb contents. The excess of Ti in the liquid is responsible for the formation of Ti<sub>2</sub>Ni. Higher amounts of Nb, as observed in Nb10, hinder the formation of Ti<sub>2</sub>Ni, favoring β-Ti at high temperatures. The decrease in Ni content and accumulation of Nb are associated with the formation of the eutectic involving β-Nb. In the final stages of solidification, Ti<sub>2</sub>Ni and the eutectic form simultaneously when the Ni content reaches a critical level. TiNi, β-Nb and Ti<sub>2</sub>Ni are equilibrium phases in Ti-rich regions in TiNi – Nb pseudobinaries, which can be related to a high stability of these phases.

From element distribution analyses, it has been observed that coherent ratios are obtained in the intermetallic phases when Cu is considered a substitute for Ni, and Nb, for Ti. These results endorse that Nb occupy Ti sites. Cu is always present as a solute, preferably in the TiNi formed in the final stages of solidification while Nb precipitates as β-Nb.

#### 5. Acknowledgments

This work was partially supported by Conselho Nacional de Desenvolvimento Científico e Tecnológico (CNPq) – Grant number 432329/2018-8; Coordenação de Aperfeiçoamento de Pessoal de Nível Superior (CAPES/PROEX) – Finance code 001; Fundação de Amparo à Pesquisa de Minas Gerais (FAPEMIG); Pro-Reitoria de Pesquisa da Universidade Federal de Minas Gerais (PRPq – UFMG). The authors would like to thank the Companhia Brasileira de Metalurgia e Mineração (CBMM) for the donation of Nb and the Centro de Microscopia da UFMG.

#### 6. References

- Otsuka K, Wayman CM. *Shape memory materials*. Cambridge: Cambridge University Press; 1998. 284 p.
- Otsuka K, Ren X. Martensitic transformations in nonferrous shape memory alloys. *Mater Sci Eng A*. 1999;273–275:89-105.
- Otsuka K, Ren X. Physical metallurgy of Ti–Ni-based shape memory alloys. *Prog Mater Sci*. 2005;50:511-678.
- Wollants P, Roos JR, Delaey L. Thermally and stress-induced thermoelastic martensitic transformations in the reference frame of equilibrium thermodynamics. *Prog Mater Sci*. 1993;37:227-88.
- Chen X, Srivastava V, Dabade V, James RD. Study of the cofactor conditions: conditions of supercompatibility between phases. *J Mech Phys Solids*. 2013;61(12):2566-87. <http://dx.doi.org/10.1016/j.jmps.2013.08.004>.
- Zhang Z, James RD, Muller S. Energy barriers and hysteresis in martensitic phase transformations. *Acta Mater*. 2009;57(147):4332-52.
- Nam TH, Saburi T, Nakata Y, Shimizu K. Shape memory characteristics and lattice deformation in Ti–Ni–Cu alloys. *Mater Trans JIM*. 1990;31(12):1050-6.
- Nam TH, Saburi T, Shimizu K. Cu-content dependence of shape memory characteristics in Ti–Ni–Cu Alloys. *Mater Trans JIM*. 1990;31(11):959-67.
- Moumni Z, Van Herpen A, Riberty P. Fatigue analysis of shape memory alloys: energy approach. *Smart Mater Struct*. 2005;14(5):S287.
- Gall K, Maier HJ. Cyclic deformation mechanisms in precipitated NiTi shape memory alloys. *Acta Mater*. 2002;50:4643-57.
- Kato H, Ozu T, Hashimoto S, Miura S. Cyclic stress-strain response of superelastic Cu–Al–Mn alloy single crystals. *Mater Sci Eng A*. 1999;264(1–2):245-53.
- Tsuji K, Takegawa Y, Kojima K. Thermal fatigue characteristics of NiTiCu alloy coils. *Mater Sci Eng A*. 1991;136(C):1-4.
- Wei ZG, Miyazaki S, Tang W, Sandstro R. Experimental investigation and thermodynamic calculation of the Ti–Ni–Cu shape memory alloys. *Metall Mater Trans, A Phys Metall Mater Sci*. 2000;31:2423-30.
- Shim JH, Kim JH, Lim JH, Kim JG, Oh JS, Lee T, et al. Improvement in the superelasticity of a Ti–35.5Ni–15Cu (at.%) alloy using Ti(Ni,Cu)<sub>2</sub> phase. *Mater Sci Eng A*. 2022;847:143346.
- Roy ASN, Narendranath S. Impact of variation in wire electro discharge machining responses of homologous TiNiCu shape memory alloys for smart applications: an experimental investigation. *Mater Res Express*. 2018;5(12):125701.
- Villa F, Nespoli A, Passaretti F, Villa E. Microstructural and thermo-mechanical characterization of cast niticu20 shape memory alloy. *Materials (Basel)*. 2021;14(14):3737.



17. Zheng HX, Mentz J, Bram M, Buchkremer HP, Stöver D. Powder metallurgical production of TiNiNb and TiNiCu shape memory alloys by combination of pre-alloyed and elemental powders. *J Alloys Compd.* 2008;463(1-2):250-6.
18. Pan G, Balagna C, Martino L, Pan J, Spriano S. Microstructure and transformation temperatures in rapid solidified Ni – Ti alloys. Part II : the effect of copper addition. *J Alloys Compd.* 2014;589:633-42. <http://dx.doi.org/10.1016/j.jallcom.2013.09.212>.
19. Jin B, Lu X, Liu S, Xu K, Du Y, Zhang S, et al. Thermodynamic re-assessment and liquidus projection of the Cu–Ni–Ti system. *Calphad.* 2021;73:102256.
20. Zhang H, He Y, Yang F, Liu H, Jin Z. Thermodynamic assessment of Cu-Ni-Ti ternary system assisted with key measurements. *Thermochim Acta.* 2013;574:121-32. <http://dx.doi.org/10.1016/j.tca.2013.08.012>.
21. Zhu WJ, Duarte LI, Leinenbach C. Experimental study and thermodynamic assessment of the Cu-Ni-Ti system. *Calphad.* 2014;47:9-22. <http://dx.doi.org/10.1016/j.calphad.2014.06.002>.
22. Wang GC, Hu KP, Tong YX, Tian B, Chen F, Li L, et al. Influence of Nb content on martensitic transformation and mechanical properties of TiNiCuNb shape memory alloys. *Intermetallics.* 2016;72:30-5.
23. Tong Y, Gu H, James RD, Qi W, Shuitcev AV, Li L. Novel TiNiCuNb shape memory alloys with excellent thermal cycling stability. *J Alloys Compd.* 2019;782:343-7.
24. Zhou X, Huang Z, Chen F, Tian B, Li L, Tong Y. Two-way shape memory effect with excellent cycling stability in TiNiCuNb alloy. *Mater Lett.* 2021;2022(308):2021-3.
25. Liu MY, Qi WY, Tong YX, Tian B, Chen F, Li L. Study of martensitic transformation in TiNiCuNb shape memory alloys using dynamic mechanical analysis. *Vacuum.* 2018;155:358-60.
26. Silva JD, Macieira GF, Santos DS, Santos L A, Buono VTLB. Role of Nb on the phase stability and morphology of Ti-Ni-Cu-Nb alloys. *J Mater Res Technol.* 2022;20:1428-36. <http://dx.doi.org/10.1016/j.jmrt.2022.07.146>.
27. Lukas HL, Fries SG, Sundman B. Computational thermodynamics: the calphad method. Cambridge: Cambridge University Press; 2007.
28. Chen Q, Sundman B. Computation of partial equilibrium solidification with complete interstitial and negligible substitutional solute back diffusion. *Mater Trans.* 2002;43(3):551-9.
29. Schaffnit P, Stallybrass C, Konrad J, Stein F, Weinberg M. A Scheil-Gulliver model dedicated to the solidification of steel. *Calphad.* 2015;48:184-8. <http://dx.doi.org/10.1016/j.calphad.2015.01.002>.
30. Samal S, Biswas K, Phanikumar G. Solidification behavior in newly designed Ni-Rich Ni-Ti-Based alloys. *Metall Mater Trans, A Phys Metall Mater Sci.* 2016;47(12):6214-23.
31. Zhang Y, Hu B, Zeng G, Liu S, Du Y, Yin H. Experimental investigation, thermodynamic modeling and solidified microstructure of the Cu–Ti–Nb ternary system. *Calphad.* 2022;76:102395. <http://dx.doi.org/10.1016/j.calphad.2022.102395>.
32. Chen SL, Yang Y, Chen SW, Lu XG, Chang YA. Solidification simulation using scheil model in multicomponent systems. *J Phase Equilibria Diffus.* 2009;30(5):429-34.
33. Chang K, Liu S, Zhao D, Du Y, Zhou L, Chen L. Thermodynamic description of the Al-Cu-Mg-Mn-Si quinary system and its application to solidification simulation. *Thermochim Acta.* 2011;512(1-2):258-67. <http://dx.doi.org/10.1016/j.tca.2010.11.009>.
34. Shi H, Frenzel J, Martinez GT, Van Rompaey S, Bakulin A. Site occupation of Nb atoms in ternary Ni – Ti – Nb shape memory alloys. *Acta Mater.* 2014;74:85-95. <http://dx.doi.org/10.1016/j.actamat.2014.03.062>.